ISBN: 978-3-95450-132-8 doi:10.18429/JACoW-IPAC2014-THPRO034

DESIGN OF THE LCLS-II ELECTRON OPTICS *

Y. Nosochkov†, P. Emma, T. Raubenheimer, M. Woodley, SLAC, Menlo Park, CA 94025, USA

Abstract

The LCLS-II project is a high repetition rate, high average brightness free-electron laser based on the existing facilities at the SLAC National Accelerator Laboratory. The LCLS-II will be driven by a new CW superconducting RF (SCRF) 4-GeV linac replacing the existing Cu-linac in the 1st km of the linac tunnel. The SCRF linac will include chicanes for providing full compression of the electron bunch length. After the linac, the electron beam will be directed into the existing 2-km bypass line connecting to the Beam Switch Yard (BSY), where a new spreader system will allow a high rate bunch-by-bunch deflection into the hard X-ray (HXR) or soft X-ray (SXR) transport lines, or towards the BSY high power dump. The HXR line will include a new variable gap undulator replacing the existing LCLS-I undulator and will reuse the existing LCLS-I linac-to-undulator and dump transport lines. The SXR will require a new transport line sharing the same tunnel with the HXR and will include a new variable gap undulator. Overview of the electron beam transport and the optics design are presented.

INTRODUCTION

The LCLS-II project is a high repetition rate, high average brightness free-electron laser (FEL) based on the LCLS-I [1] and existing facilities at the SLAC National Accelerator Laboratory. Schematic of the LCLS-II horizontal layout along with the LCLS-I is shown in Fig. 1.

The project includes a new high repetition rate (MHz) injector and a Continuous Wave (CW) superconducting RF (SCRF) 4-GeV linac, replacing the existing Cu-linac in the 1st km of the linac tunnel. The electron bunches will be compressed using compressor chicanes in the linac. Then the beam will be transported through the existing 2-km long bypass line to the Beam Switch Yard (BSY), where a new 3-way spreader system will be installed. It will provide high rate bunch-by-bunch deflection either into SXR (soft X-ray) or HXR (hard X-ray) lines, or towards the BSY high power dump. The beams then will be transported to the existing LCLS-I undulator hall where new SXR and HXR variable gap undulators will be installed. The transport from the BSY to the HXR undulator will reuse the existing LCLS-I linac-to-undulator (LTUH) beamline, while the transport from the BSY to the SXR will require a new LTUS beamline. The facility will also provide beam delivery from the existing LCLS-I 120-Hz Cu-linac to the new HXR undulator. Optics design for the LCLS-II electron transport lines using MAD [2] is described below.

* Work supported by the Department of Energy Contract DE-AC02-76SF00515.
† yuri@slac.stanford.edu

SCRF LINAC

Schematic of the new 4-GeV SCRF linac and parameters are shown in Fig. 2. The design will be based on existing technology developed for TESLA [3], ILC [4] and XFEL [5]. The linac includes 35 1.3-GHz cryomodules (CM) in the four main linac sections (L0, L1, L2, L3), a laser heater chicane (LH), a harmonic linearizer RF section (HL), and two bunch compressor chicanes (BC1, BC2). There is one 12-m long CM in L0, two in L1, 12 in L2, and 20 in L3. The last two CMs in L3 (named Lf) will be used for energy feedback. The main CM includes eight 9-cell cavities (each $\simeq$ 1 m long) resonant at 1.3-GHz, while the 3.9-GHz HL consists of two CMs, each comprising of eight shorter 9-cell cavities. The average accelerating gradient is under 16 MV/m, where $\simeq$ 6% of cavities are not powered, serving as spares. The L3 cavities run on crest ($\phi = 0$) since the resistive-wall wake-field of the downstream 2-km bypass line removes the remnant energy chirp on the bunch. At the end of the SCRF linac, a linac extension section is reserved for future energy upgrade. The latter transports the beam for $\simeq$250 m to Sector-10 in the SLAC tunnel at which point the beam is directed up into the existing 2-km bypass line. There will be offset diagnostic lines just after the laser heater and the BC1 into which the beam will be continuously deflected at a low rate (~100 Hz). These lines will include transverse deflecting cavities (TCAV) for an ongoing analysis of the beam slice emittance and longitudinal phase space.

Lattice functions of the main linac, the downstream extension section, and bypass dogleg are shown in Fig. 3. The 30° FODO lattice in L2 and L3 uses cold quadrupole magnets at the end of each CM. Several warm quadrupoles around the bunch compressors provide a proper match of beta functions at these locations. This relatively weak FODO optics helps reducing chromatic effects and loosens alignment tolerances and dispersion errors. The downstream extension section is made of 38-m long 90° FODO cells.

In order to drive the FELs, the 100-pC electron bunch length must be compressed by a factor of 100 to provide 1 kA of peak current. This is achieved with two four-bend compressor chicanes BC1 and BC2 and a linear energy chirp on the bunch induced by off-crest RF phasing. A third optional chicane (BC3) is also included. The BC1 chicane is placed close to the injector, but at high enough energy (250 MeV) so that space charge forces do not degrade the beam brightness. The 3.9-GHz HL section before the BC1 removes the 2nd order chirp curvature. The BC2 chicane is placed at 1.6 GeV such that the remaining linear energy chirp (after compression) is canceled by the longitudinal wake-field of the accelerating cavities and the resistive-wall wake-field of the bypass line. The R_{56} values of BC1 and BC2 are set to -55 mm and -37 mm, respectively, for optimal compression and minimal impact on the transverse emittance. The optional

ISBN: 978-3-95450-132-8 doi:10.18429/JACoW-IPAC2014-THPRO034

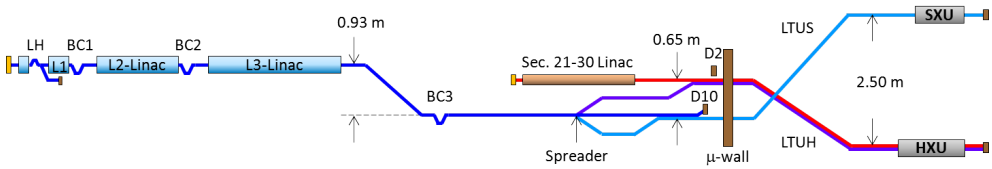

Figure 1: Schematic top view of the LCLS-II and LCLS-I (not to scale).

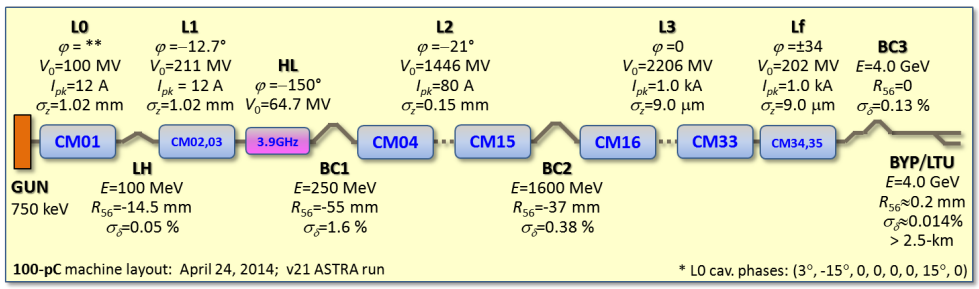

Figure 2: Schematic and parameters of the LCLS-II SCRF linac.

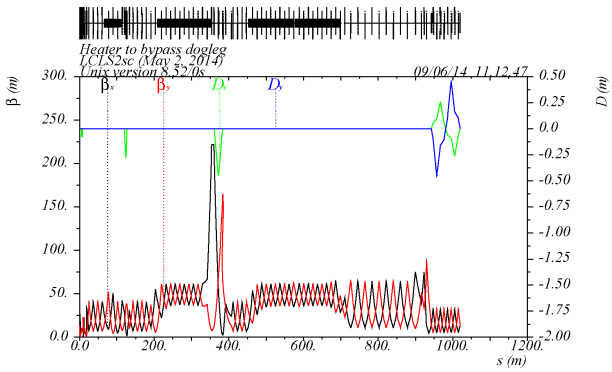

Figure 3: LCLS-II beta functions and dispersion from injector to bypass dogleg.

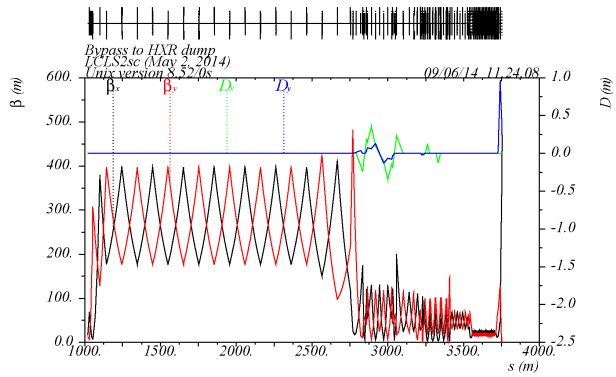

Figure 5: LCLS-II beta functions and dispersion from bypass to HXR dump.

BC3 chicane (nominally turned off) is placed at 4 GeV just before the bypass. Effects of coherent synchrotron radiation generated in the chicane bends are minimized by forcing a small horizontal beta function at the last chicane bend, see e.g. BC2 optics in Fig. 4.

DOWNSTREAM TRANSPORT

At the end of the linac extension section the beam enters a bypass dogleg directing the beam into the existing bypass line located 1.64 m up and 0.93 m to the right of the SCRF linac axis. The dogleg is made of two rolled bend magnets separated by four 90° FODO cells providing dispersion cancelation. This is followed by a four quadrupole matching section containing the BC3 and connecting to the bypass line. The optics from the beginning of bypass to the HXR dump is shown in Fig. 5. The bypass is a long 2-inch diameter stainless steel cylindrical pipe which includes one quadrupole, BPM, and steering coils every 101.6 m. The large quadrupole spacing leads to high beta functions (up to 400 m) with 45° FODO cells. This line includes four wires for emittance measurement at low beam power and two horizontal and two vertical adjustable-gap collimators for removing beam tails before the undulator.

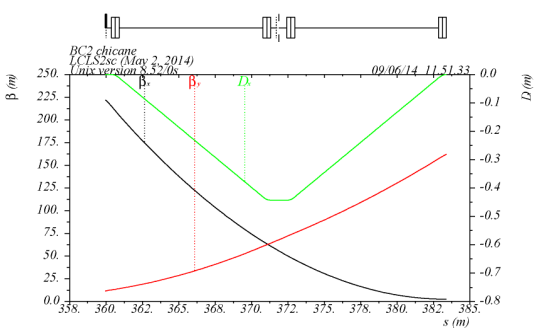

Figure 4: Lattice functions of the LCLS-II BC2 chicane.

At the end of the bypass in Sector-28, a 3-way vertically deflecting device (spreader), based on magnetic kicker or RF deflector [6, 7], will provide a high-rate bunch-by-bunch deflection into separate SXR or HXR transport lines, or to the existing high power BSY dump D10 (250 kW). After the spreader, the beams will enter a three-hole Lamberston septum magnet where the small vertical kick from the spreader (±0.75 mrad or 0) is used to select a much stronger left or

ISBN: 978-3-95450-132-8 doi:10.18429/JACoW-IPAC2014-THPRO034

right horizontally bending field (for HXR and SXR branches) or no field (for BSY dump line) to fully separate the beams. Horizontal layout of the spreader system is shown in Fig. 6. Note that the LCLS-I linac in this Figure is ≃65 cm below the LCLS-II bypass. The SXR branch remains at the bypass level in this region, and the HXR and the dump branches descend to the LCLS-I level.

The HXR line from the spreader is connected to the existing LCLS-I line in the BSY using a 2-step dogleg, where the two outer bends are horizontal, and the two inner bends are rolled providing both x and y bending. The included quadrupoles match the beta functions and cancel dispersion and R_{56} created by the dogleg bends. Two vertical corrector bends cancel vertical trajectory and dispersion created by the spreader kick. The HXR spreader optics, including the downstream part of the BSY, is shown in Fig. 7. The existing LCLS-I may still be used to feed the HXR undulator at 3-15 GeV and 120-Hz repetition rate by switching off the last bend of the HXR spreader dogleg.

To provide sufficient separation from the other lines, the SXR branch of the spreader uses a 4-bend symmetric chicane with quadrupoles. The latter match the beta functions and cancel horizontal dispersion and R_{56} generated by the chicane bends. A small vertical trajectory and dispersion created by the spreader kick is canceled by two vertical corrector bends. Finally, when there is no kick from the spreader, the beam goes through a zero-field hole in the septum and then directed to the BSY high power dump D10 located at the level of LCLS-I. This is achieved with two quadrupoles, 2-bend vertical dogleg and one horizontal bend.

After the spreader, the HXR beam will enter the existing LTUH line that will connect to the new HXR undulator. This line consists of a horizontal dogleg providing 1.25-m offset, and 45° FODO optics for 4-wire emittance diagnostics. A new LTUS beamline will be constructed for the SXR beam that leads from the BSY to the SXR undulator. It will include a 2-bend horizontal dogleg providing 1.90-m offset and similar diagnostic section as in HXR. Both LTUH and LTUS include weak vertical bends which remove the intrinsic SLAC linac downward slope and place the HXR and SXR undulators at the same vertical level while being 2.5-m apart horizontally. Beam halo and energy collimators are included in the BSY and LTUH, LTUS regions.

The new HXR and SXR undulator sections will include variable gap permanent magnet hybrid undulators installed

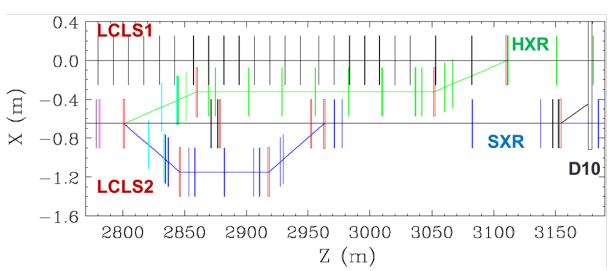

Figure 6: Top view of the LCLS-II spreader including the LCLS-I line.

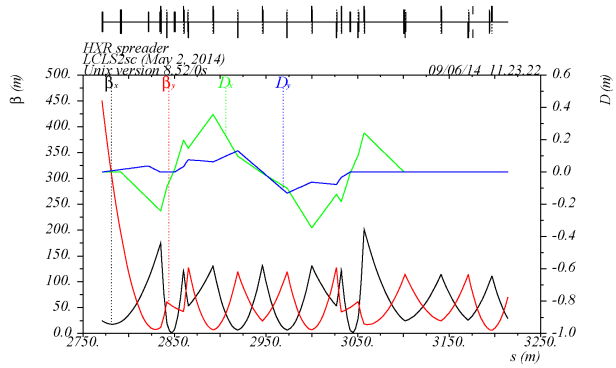

Figure 7: Lattice functions of the HXR spreader.

in the existing LCLS-I undulator hall. The undulator sections will be composed of 4.4-m long cells each containing a 3.4-m undulator segment and 1.0-m break section consisting of a quadrupole, phase shifter, RF BPM, a beam loss monitor, and steering coils. Limited by the length of the undulator hall, the HXR will include 32 undulator cells and 2 cells for self-seeding monochromators. With the selected 26-mm period and 7.2-mm gap, the HXR undulator will be able to support self-seeded operation up to 4 keV at 4 GeV electron energy. The SXR will include 21 undulator cells and one cell for self-seeding monochromator. With the 39-mm period and 7.2-mm gap, it will support self-seeding over photon energy range of 0.2 to 1.3 keV. Since the HXR and SXR sections are of equal length, the remaining unused 12 cells of the SXR are reserved for future undulator extension, containing just four quadrupoles for the lattice match in the nominal design. The undulator quadrupoles make FODO optics with an average beta function of ≃12 m in SXR and 20 m in HXR at nominal conditions.

The undulator sections are followed by the HXR and SXR main dump lines. They use 3.9° vertical bends which are rolled 10° to direct the discarded beams in a downward direction while horizontally converging to allow more efficient shielding in the existing tunnel. A "soft" vertical bend upstream of the main bends redirects coherent edge radiation from the main bends away from the downstream experiments. The three dump line quadrupoles provide proper optics with large vertical dispersion and small vertical beta function at an OTR screen for measurements of electron beam energy spread. The HXR line will reuse the existing X-band TCAV deflector for time-resolved diagnostic. This measurement is also planned for the SXR line.

REFERENCES

[1] P. Emma, *et al.*, Nature Photonics, **4**, 641-647 (2010).
[2] MAD, http://mad.web.cern.ch/mad
[3] http://tesla.desy.de/new_pages/TDR_CD/start.html
[4] http://www.linearcollider.org/
[5] http://www.xfel.eu/
[6] M. Placidi, *et al.*, IPAC 2013, WEPWA069 (2013).
[7] M. Placidi, *et al.*, NGLS Tech. Note 0036 (2013).